Magnetoelastic coupling in $DyMn_2O_5$ via infrared spectroscopy

J. Cao,[1,*] L. I. Vergara,[1] J. L. Musfeldt,[1] A. P. Litvinchuk,[2] Y. J. Wang,[3] S. Park,[4] and S.-W. Cheong[4]
[1]*Department of Chemistry, University of Tennessee, Knoxville, Tennessee 37996, USA*
[2]*Texas Center for Superconductivity and Department of Physics, University of Houston, Houston, Texas 77204, USA*
[3]*National High Magnetic Field Laboratory, Florida State University, Tallahassee, Florida 32310, USA*
[4]*Rutgers Center for Emergent Materials and Department of Physics and Astronomy, Rutgers University, Piscataway, New Jersey 08854, USA*
(Received 10 June 2008; published 26 August 2008)

We investigated the infrared-active phonons in $DyMn_2O_5$ as a function of temperature and magnetic field in order to elucidate the magnetic ordering-induced lattice distortions. Spin-lattice coupling in this geometrically frustrated multiferroic is evidenced by small frequency shifts of several phonon modes at various magnetic ordering temperatures, vibrational frequency shifts between 60 and 65 K from which we extract large coupling constants, and magnetic-field dependence of numerous phonons. We analyze these results in terms of local lattice distortions and discuss the consequences for the ferroelectric polarization and magnetodielectric effect.

DOI: 10.1103/PhysRevB.78.064307 PACS number(s): 75.47.Lx, 75.80.+q, 78.20.Ls, 78.30.−j

I. INTRODUCTION

The interplay between spin, lattice, charge, and orbital degrees of freedom drives rich physics in complex oxides. Because these interactions are so strong, oxides are on the "knife's edge," straddling several unique regions in physical (pressure-temperature-field) and chemical phase space. An important consequence of this multiphase proximity is the physical property tunability and, in some cases, the opportunity to drive new functionality. Although the overall role of the lattice is commonly acknowledged in these processes, little is known about magnetic ordering-induced lattice distortions or the effect of high magnetic field on local structure. It has generally been assumed that the lattice is rigid, with potential coupling limited by the different energy scales of magnetic and vibrational processes. Recent investments in new facilities and experiments on a wide variety of materials are, however, starting to yield a different consensus. Magnetostriction measurements and work on shape-memory materials currently provide the strongest evidence for a flexible crystalline lattice.[1–8] At the same time, vibrational spectroscopies are beginning to demonstrate that specific information on local lattice displacements can be correlated with magnetic ordering transitions.[9,10] A few examples of magnetic-field dependent phonons are also starting to emerge, although the effects are generally small.[11–15] Materials with strong spin-phonon coupling (such as the multiferroics) offer a way to investigate potentially much larger effects.

We focused our search for sizable magnetoelastic coupling on geometrically frustrated $DyMn_2O_5$ [Fig. 1(a)].[7,16–20] At 300 K, it displays an orthorhombic *Pbam* crystal structure consisting of distorted $Mn^{4+}O_6$ octahedra that share edges along the *c* axis. Distorted $Mn^{3+}O_5$ square pyramidal units link the edge-sharing octahedral chains together. The Mn^{3+} ($S=2$) and Mn^{4+} ($S=3/2$) spins are geometrically frustrated, leading to a degenerate ground state that can be lifted by lattice distortion.[18] $DyMn_2O_5$ displays a rich magnetic field-temperature phase diagram with a cascade of magnetic transitions and a series of magnetic phases. The critical fields depend on the direction of the applied field.[7,21,22] Antiferromagnetic order with an incommensurate magnetic modulation develops at $T_{N1}=43$ K followed by a lock-in transition at $T_{C1}=39$ K into a commensurate ferroelectric (FE) phase.[7,21,22] The Mn^{3+} and Mn^{4+} spins reorient further at $T_{N2}=27$ K and $T_{C2}=18$ K.[7,21,22] The system re-enters an incommensurate magnetic state at $T_{C3}=6.5$ K, which coincides with the ordering of Dy^{3+} moments.[7,22] Bulk magnetoelastic measurements at 4.2 K show that the transition fields are $H_{C3}\sim 1.5$ T (PE$\rightarrow$FE3, $H\|a$ or $H\|b$), $H_{HF}\sim 4$ T (PE$\rightarrow$HF, $H\|c$), and $H_{C2}\sim 8.5$ T (FE3$\rightarrow$FE2, $H\|b$).[7] Here, PE and HF refer to paraelectric and high field, respectively. Large hysteresis effects are observed. Although magnetostriction, thermal expansion, heat capacity, and dielectric constant measurements demonstrate changes in average structure, unit-cell lattice constants, and bulk phonon contributions,[7,17,23,24] they do not provide specific information on the most important local lattice displacements (i.e., bond length and angle changes) and how they differ in various magnetic states.

In order to elucidate possible magnetic ordering-induced lattice distortions and the effect of high magnetic field on phonon modes in a material with strong spin-lattice interactions, we investigated the infrared spectral response of multiferroic $DyMn_2O_5$ as a function of temperature and magnetic field. Complementary lattice dynamics calculations were carried out to determine frequencies and displacement patterns of vibrational modes. Spin-lattice mixing is evidenced by the substantial frequency shifts between 60 and 65 K from which we extract coupling constants and smaller vibrational frequency shifts at several magnetic ordering temperatures. The majority of vibrational modes are sensitive to magnetic field, indicating that the applied field modifies inter-ionic interactions and local structure by distorting the quasioctahedral and pyramidal building block units, both locally and with respect to the Dy^{3+} centers.[15] In this work we focus on three low-frequency modes near 100 cm^{-1} and demonstrate that relative Dy^{3+}/manganese oxide polyhedral displacements drive the PE$\rightarrow$HF ($H\|c$) at 4 T. That spin-lattice interactions can be probed by direct vibrational property measurements and mediated by temperature or an ap-

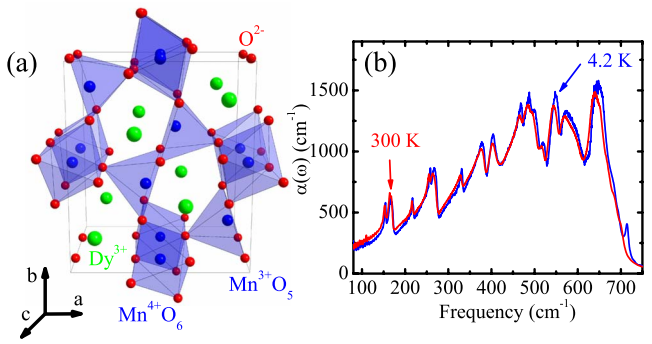

FIG. 1. (Color online) (a) 300 K crystal structure of geometrically frustrated $DyMn_2O_5$ showing distorted $Mn^{4+}O_6$ ($S=3/2$) octahedra cross linked with distorted $Mn^{3+}O_5$ ($S=2$) square pyramids.[20] (b) Absorption spectrum of $DyMn_2O_5$.

plied magnetic field has important consequences for the design of functional oxides, where many exotic properties derive from a flexible lattice and strong spin-lattice-charge mixing rather than a rigid lattice and separation of the different degrees of freedom.

II. METHODS

Single crystals of $DyMn_2O_5$ were grown using B_2O_3-PbO-PbF_2 flux in a Pt crucible and characterized by magnetization, polarization, and x-ray diffraction. Small pieces were mixed with paraffin or KCl powder to form isotropic pellets for unpolarized transmittance measurements in far and middle infrared regimes, respectively. Our variable-temperature infrared transmittance measurements were performed using a series of Fourier transform infrared spectrometers covering the frequency range from 30 to 7500 cm^{-1} with 0.5 cm^{-1} resolution.[15] The absorption coefficient was obtained from the measured transmittance as $\alpha=-\frac{1}{hd}\ln T$, where h is the loading of $DyMn_2O_5$ in the pellet and d is the pellet thickness. Magnetoinfrared transmittance measurements were carried out at the National High Magnetic Field Laboratory in Tallahassee, FL using an 18 T superconducting magnet.[15] Field-induced changes in the measured transmittance were studied by taking the ratio of transmittance at high field and transmittance at zero field, i.e., $T(H)/T(H=0\ \mathrm{T})$. We renormalized the high-field transmittance ratios to the zero-field absolute transmittance spectra and recalculated the absorption coefficient α. To emphasize the changes with magnetic field, we also calculated the absorption difference spectra $[\alpha(H)-\alpha(0\ \mathrm{T})]/\alpha(0\ \mathrm{T})$. We quantify field-induced changes in the absolute absorption difference as $\int_{\omega_0}^{\omega_1}|\frac{\Delta\alpha}{\alpha}|d\omega$, where ω_0 and ω_1 define the frequency range of interest. Lattice dynamical calculations were performed within the shell model using the general utility lattice program[25] along with the $DyMn_2O_5$ crystallographic data reported in Ref. 20.

III. RESULTS AND DISCUSSION

A. Vibrational mode assignments and temperature effects

Figure 1(b) displays the absorption spectrum of $DyMn_2O_5$ at 300 and 4 K. The observed peaks are assigned via comparison with our lattice dynamics calculations (Table I) and are in excellent agreement with *ab initio* results reported in Refs. 27 and 28. The modes predicted to be between 283 and 762 cm^{-1} are due to Mn-O stretching and bending motions of the distorted octahedra and square pyramids. The lower energy features, calculated to be between 95 and 245 cm^{-1}, are mainly due to the relative motion of Mn-containing polyhedra and Dy^{3+} ions. Group theory predicts 36 infrared-active vibrational modes in the paraelectric phase of $DyMn_2O_5$ at the Γ point $[\Gamma_{IR}=14B_{3u}(E\|a)+14B_{2u}(E\|b)+8B_{1u}(E\|c)]$. With the exception of small frequency shifts through the magnetic transitions (discussed below), the spectrum just above T_{N1} is nearly identical to that at 4.2 K. No symmetry breaking is observed through the cascade of magnetic transitions.[26] This is in agreement with recent calculations indicating that atomic displacements that lower the structural symmetry to the noncentrosymmetric group are very small.[27,28] In addition to infrared-active phonons, the experimental spectrum may also contain rare-earth crystal-field excitations.[29–31]

TABLE I. Comparison of calculated phonon modes and experimental peak frequencies for $DyMn_2O_5$. All frequencies are in cm^{-1}.

B_{3u}(a)	B_{2u}(b)	B_{1u}(c)	Experimental range
95	104	117	95–110
170	176		140–180
189	184		
208			217
	231	245	230–260
	283		267
310			290
336	339	325	310–350
382	387	368	350–385
403			403
	441	456	430–470
475	464	473	470–510
486	475		
		509	519
567	576		530–555
585	589		555–600
617	626	655	610–670
	728		680
762			713

Figure 2 displays the peak positions of several features in the absorption spectrum of $DyMn_2O_5$ as a function of temperature along with representative mode displacement patterns obtained from our dynamics calculations and assigned to the spectral features of interest in the associated panels. With decreasing temperature, all phonon modes harden. In order to distinguish this natural anharmonicity from more subtle effects that occur at the low-temperature magnetic transitions, we fit the temperature dependence of the mode frequencies[32] between 300 and 60 K as

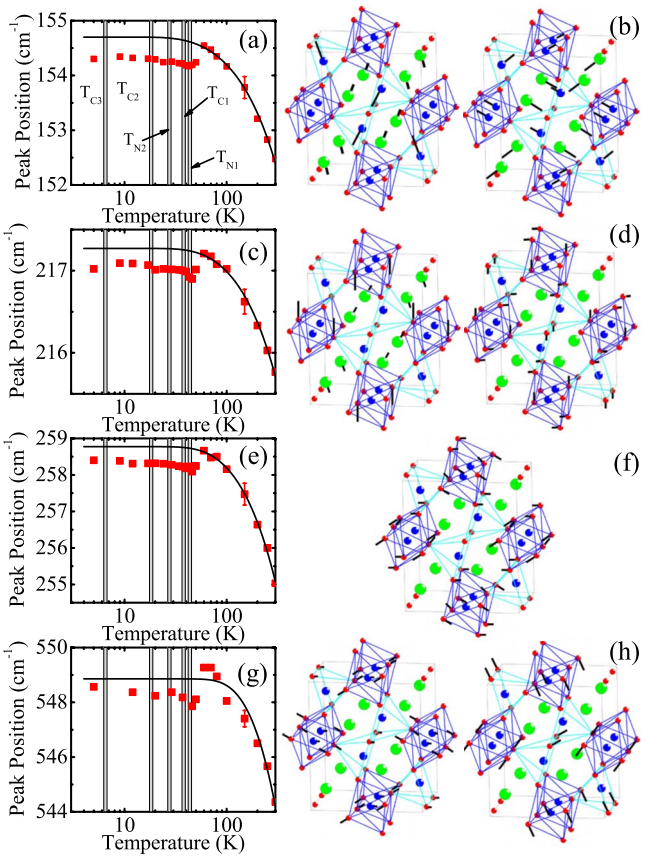

FIG. 2. (Color online) Panels (a), (c), (e), and (g): Peak positions of representative features in the vibrational spectrum of $DyMn_2O_5$ as a function of temperature. The solid lines are fits to the high-temperature anharmonic response [Eq. (1)]. The gray vertical lines denote magnetic transition temperatures (Ref. 7) and are labeled in (a). Panels (b), (d), (f), and (h) representative mode displacement patterns of $DyMn_2O_5$, as obtained from our molecular-dynamics calculations for the modes with calculated frequencies at 170 and 176 cm^{-1} in (b), 208 and 231 cm^{-1} in (d), 283 cm^{-1} in (f), and 567 and 576 cm^{-1} in (h).

$$\omega_m(T) = \omega_{0m} - C_m\left[1 + \frac{2}{\exp(\hbar\omega_{0m}/2k_BT) - 1}\right]. \quad (1)$$

Here, ω_{0m} represents the frequency of mode m in the absence of spin-phonon coupling and C_m is a mode-dependent scaling factor for anharmonic contributions. As shown in the left-hand panels of Fig. 2, this model provides a good fit to the high-temperature phase data.

The peak position vs temperature data deviate from purely anharmonic behavior upon approach to T_{N1} (and in the low-temperature range where the lattice is overall softer). Near 60 K, all infrared-active vibrational features of $DyMn_2O_5$ soften. Some modes soften substantially. In contrast, the 633 and 706 cm^{-1} Raman-active Mn-O stretching modes in $DyMn_2O_5$ harden, although these same modes soften in other RMn_2O_5 compounds.[33] Anomalous phonon shifts at T^* ($\sim$60–65 K) and near the Néel temperature (T_{N1}) have been observed in other rare-earth manganites and are attributed to spin-phonon coupling effects.[33–36] Upon cooling through T_{N1}, the infrared-active vibrational modes of $DyMn_2O_5$ display weak dips. In addition to changes at 43 K, selected modes (such as the 155, 217, 258, and 548 cm^{-1} features) display weak inflections at the spin reorientation temperature T_{N2} (27 K) and the combined lock–in/spin reorientation temperature T_{C2} (18 K). This indicates that the three different FE phases are associated with slightly different phonon characteristics, although as predicted,[28] the magnetic ordering-induced lattice distortions are small. The transition from FE1 $\rightarrow$ FE2 at T_{N2} is associated with a modest change in the Mn-O stretching modes of the octahedra and square pyramids and relative motion of the polyhedra and Dy^{3+} centers, whereas the transition from FE2 $\rightarrow$ FE3 at T_{C2} is accompanied by these same distortions plus changes in Mn-O bending modes and relative motion of the Dy^{3+} and O centers. Within our sensitivity and spectral resolution, there is no mode splitting at any of these low-temperature magnetic transitions. This is different from $TbMn_2O_5$, where a weak b polarized Raman-active phonon in the paraelectric phase becomes infrared active at the ferroelectric transition due to loss of inversion symmetry.[9]

We analyze the mode softening between T^* and T_{N1} in terms of the spin-phonon coupling process.[35,37–40] The phonon frequency is sensitive to spin correlations as

$$\omega_m = \omega_m^0 + \lambda_m\langle \mathbf{S}_i \cdot \mathbf{S}_j\rangle, \quad (2)$$

where $\langle \mathbf{S}_i \cdot \mathbf{S}_j\rangle$ is the nearest-neighbor spin-spin correlation function and λ_m is the coupling constant for the mth mode. In order to extract λ_m, it is necessary to estimate a reasonable value of $\langle \mathbf{S}_i \cdot \mathbf{S}_j\rangle$ or measure it by inelastic neutron scattering. One way to estimate the spin-spin correlation function is to employ mean-field theory and cluster expansion techniques to calculate the short-range order parameter $\phi(T) = |\langle \mathbf{S}_i \cdot \mathbf{S}_j\rangle|/S^2$.[38] For FeF_2 and MnF_2, which both exhibit indirect exchange, $\phi(T)$ was predicted to be $\sim$0.17 just above T_N.[38] Assuming a similar value for $DyMn_2O_5$, we can back calculate $\langle \mathbf{S}_i \cdot \mathbf{S}_j\rangle$. We find $\langle \mathbf{S}_i \cdot \mathbf{S}_j\rangle \sim -0.38$ for Mn^{4+} spins ($S = 3/2$) and ~ -0.68 for Mn^{3+} spins ($S=2$), values that could be averaged to approximately -0.5 between T^* and T_{N1} to account for the mixed valent character of this compound. We therefore calculate spin-phonon coupling constants based upon this value. Justification for this procedure is based upon the fact that the correlation function is fairly generic, with the general form depending upon the regime.[41] Each phonon in $DyMn_2O_5$ shifts differently upon approach to T_{N1}. As a result, the λ's are mode dependent. Table II summarizes spin-phonon coupling constants for several modes obtained in this fashion. The large coupling constants demonstrate that the lattice is sensitive to the magnetic state and suggest that it may respond to an applied magnetic field.

B. Magnetic-field effects

Figure 3(a) displays the magnetoinfrared absorption difference spectra of $DyMn_2O_5$ at 4.2 K. The majority of phonon modes display rich and surprisingly strong-field dependence. Many changes are on the order of $\sim$10% at 18 T and appear with complex derivative-like structure indicative of frequency shifts. In a previous report, we discussed three

TABLE II. Spin-phonon coupling constants λ_m for selected modes of $DyMn_2O_5$ estimated from the observed softening $\Delta\omega_m$ assuming $\langle \mathbf{S}_i \cdot \mathbf{S}_j \rangle \sim -0.5$. The last column gives the mode description. All frequencies, frequency differences, and coupling constants are in cm^{-1}. The large coupling constants demonstrate that the lattice is not rigid.

Mode position at 60 K (experiment)	$\Delta\omega_m$	λ_m	Mode description
154.5	0.3	0.6	
165.4	0.2	0.3	Relative motions of Mn polyhedra and Dy^{3+} ions
168.7	0.3	0.5	
217.2	0.3	0.6	Relative motions of Dy^{3+} ions and oxygens
258.7	0.5	1.0	Mn-O bending motions in MnO_6 octahedra
331.9	1.0	2.0	Mn-O twisting motions in Mn polyhedra
468.3	0.3	0.6	Mn-O bending motions within equatorial MnO_2 planes in MnO_6 octahedra
549.3	0.8	1.6	Mn-O stretching motions in MnO_6 octahedra and MnO_5 square pyramids

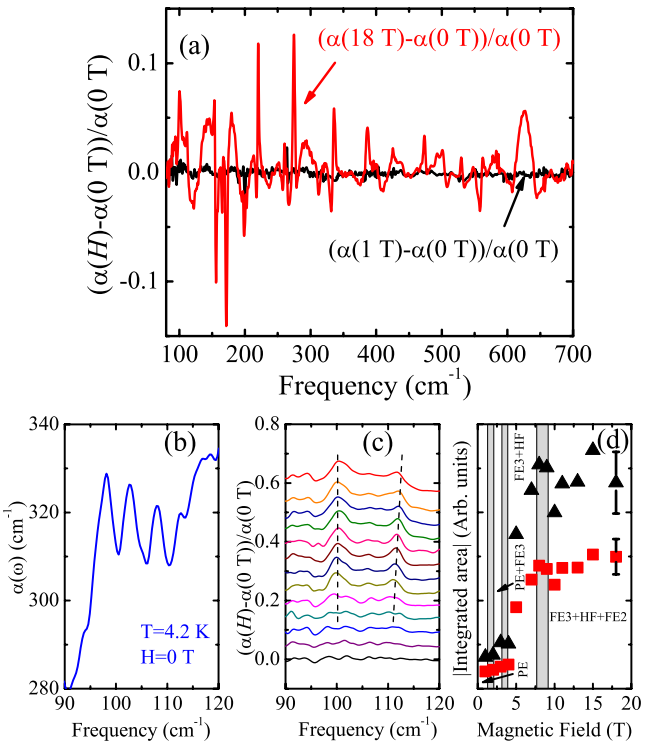

FIG. 3. (Color online) (a) Absorption difference spectra of $DyMn_2O_5$ $\{[\alpha(H)-\alpha(0\ \mathrm{T})]/\alpha(0\ \mathrm{T})\}$ at 4.2 K. (b) Close-up view of the absolute absorption spectrum at low temperature. (c) Close-up view of the absorption difference spectra near 100 cm^{-1}. The data are shown for $H=1$, 2, 3, 4, 5, 7, 8, 9, 10, 11, 13, 15, and 18 T. The curves are offset by 0.04 for clarity. (d) Integrated area of the absorption difference spectra in (c) as a function of applied magnetic field. The red squares refer to an integration range around the 100 cm^{-1} structure, whereas the black triangles refer to a slightly larger integration range (between ~95 and 115 cm^{-1}). The vertical gray lines denote various field-induced phase boundaries.[7,21]

different mode clusters as examples of the striking magneto-infrared effects observed in $DyMn_2O_5$.[15] These features (between 600 and 700 cm^{-1}, 200 and 300 cm^{-1}, and 140 and 180 cm^{-1}) were selected because they provided the best opportunity to elucidate magnetoelastic coupling effects. That the majority of vibrational modes are sensitive to magnetic field suggests that the applied field modifies local MnO_6 and MnO_5 structure and, as a consequence, affects Mn-O-Mn superexchange interactions. In addition to large λ's that facilitate field-induced modification of local structure, an applied magnetic field also drives the system through a series of magnetic ground states.[7,21] Analyzing peak positions and integrated areas of spectral features between 140 and 180 cm^{-1}, we previously demonstrated that the FE3 $\rightarrow$FE2 transition ($H \| b$) near 8.5 T is associated with changes in the lattice. The observation provides additional evidence for strong spin-lattice coupling in this system and the role of relative MnO_6 and MnO_5 polyhedra motion with respect to the Dy^{3+} centers.

It is important to extend this analysis of relative Dy^{3+} motion with respect to the metal oxide framework to include a careful examination of the three low-frequency vibrational modes near 100 cm^{-1} [Fig. 3(b)]. In addition to strong Dy^{3+} motion, these modes involve considerable Mn displacements. They are calculated to be at 95, 104, and 117 cm^{-1}, in very reasonable agreement with the experimentally observed peaks. We therefore assign these low-frequency spectral features to the relative motion of Dy^{3+} centers and manganese oxide polyhedra. The calculated displacement patterns are shown in Fig. 4.

Figure 3(c) displays a close-up view of the low-frequency absorption difference spectra of $DyMn_2O_5$. Near 4 T, small peaks emerge in $[\alpha(H)-\alpha(0\ \mathrm{T})]/\alpha(0\ \mathrm{T})$ at ~100 and 112 cm^{-1}, an observation that signals oscillator strength changes. With increasing magnetic field, the 100 cm^{-1} peak retains its position, whereas the 112 cm^{-1} feature shifts toward higher frequency. We can quantify these effects by integrating the area of the 100 cm^{-1} peak in the absorption difference spectrum or by integrating over a slightly larger

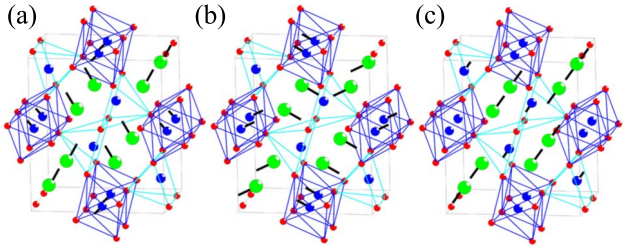

FIG. 4. (Color online) Displacement patterns for the low-frequency modes of $DyMn_2O_5$ calculated to be at (a) 95, (b) 104, and (c) 117 cm^{-1}, respectively. The predicted 117 cm^{-1} mode is purely *c* polarized.

range.[43] Plotting the integrated area as a function of applied magnetic field [Fig. 3(d)], we see that the spectral weight shows a sharp increase through 4 T, demonstrating that relative Dy^{3+}/manganese oxide polyhedral displacements participate in the PE→HF ($H\|c$) field-driven transition.

The static magnetodielectric effect in $DyMn_2O_5$ is a prominent example of the intriguing interplay between spin and lattice degrees of freedom made manifest in the bulk properties.[16] The dispersive contrast gains its strength from nearby dipole-allowed excitations. The electromagnon[42] and crystal-field excitations[30] have both been shown to contribute to this response. The magnetic-field-dependent phonons identified here (Fig. 3) and previously[15] provide additional candidates of appropriate energy and symmetry, although the relative importance of any particular excitation to the static magnetodielectric contrast decreases with increasing frequency. It is worth recalling that the trio of low-frequency modes near 100 cm^{-1} corresponding to relative Dy^{3+}/manganese oxide polyhedral displacements is sensitive to the PE→HF ($H\|c$) at 4 T, where the static magnetodielectric contrast really begins to grow. Spectral features between 140 and 180 cm^{-1} were previously associated with the FE3→FE2 transition ($H\|b$) near 8.5 T. The static magnetodielectric effect displays ≥100% contrast at 7 T but drops at higher fields, an effect that may be related to changes in the lattice at the FE3→FE2 transition.

IV. CONCLUSION

The observation that local structure is sensitive to magnetic state and applied magnetic field has important consequences for the design of functional oxides. Here, we investigated the infrared spectral response of multiferroic $DyMn_2O_5$ as a function of temperature and magnetic field, connecting important spectral features to displacement patterns using complementary dynamics calculations. This allows us to identify phonons that are coupled to the different magnetic ordering transitions. Vibrational frequency shifts are observed at several ordering transitions, and we discuss displacement patterns of some of the important modes. As in other RMn_2O_5 manganites, the largest frequency shifts are actually observed above the cascade of magnetic ordering transitions near T^* (60–65 K). We use these frequency shifts to evaluate coupling constants. Consistent with the picture of large coupling constants, strong magnetoinfrared effects are observed. Our focus on modes near 100 cm^{-1} shows that relative Dy^{3+}/manganese oxide polyhedral displacements drive the PE→HF transition at 4 T ($H\|c$). Spectral features between 140 and 180 cm^{-1} were previously shown to be associated with the FE3→FE2 transition ($H\|b$) near 8.5 T.[15] These results explain the underlying phonon contribution to many of the observed bulk property trends of $DyMn_2O_5$. Such magnetoelastic processes are not only important for multiferroic oxides but for all correlated oxides, where many exotic properties derive from spin-lattice-charge coupling rather than a rigid lattice and separation of the different degrees of freedom.

ACKNOWLEDGMENTS

This research is supported by the DOE Contract No. DE-FG02-01ER45885 (UT), Contract No. NSF-DMR-0520471 (Rutgers), the State of Texas (UH), and Contract No. NSF-DMR-0084173, DOE, and the State of Florida (NHMFL). We thank R. Valdés-Aguilar, C. J. Fennie, B. Lorenz, J. Lynn, and I. Sergienko for useful discussions.

*Materials Sciences Division, Lawrence Berkeley National Laboratory, Berkeley, California 94720, USA and Department of Materials Science and Engineering, University of California, Berkeley, California 94720, USA.

[1] T. Kimura, Y. Tomioka, A. Asamitsu, and Y. Tokura, Phys. Rev. Lett. **81**, 5920 (1998).
[2] B. García-Landa, C. Marquina, M. R. Ibarra, G. Balakrishnan, M. R. Lees, and D. McK. Paul, Phys. Rev. Lett. **84**, 995 (2000).
[3] A. N. Lavror, S. Komiya, and Y. Ando, Nature (London) **418**, 385 (2002).
[4] S. E. Russek, P. Kabos, R. D. McMichael, C. G. Lee, W. E. Bailey, R. Ewasko, and S. C. Sanders, J. Appl. Phys. **91**, 8659 (2002).
[5] H. Yamaguchi, A. K. Das, A. Ney, T. Hesjedal, C. Pampuch, D. M. Schaadt, and R. Koch, Europhys. Lett. **72**, 479 (2005).
[6] V. S. Zapf, V. F. Correa, C. D. Batista, T. P. Murphy, E. D. Palm, M. Jaime, S. Tozer, A. Lacerda, and A. Paduan-Filho, J. Appl. Phys. **101**, 09E106 (2007).
[7] C. R. dela Cruz, B. Lorenz, Y. Y. Sun, C. W. Chu, S. Park, and S.-W. Cheong, Phys. Rev. B **74**, 180402(R) (2006).
[8] Y. Boonyongmaneerat, M. Chmielus, D. C. Dunand, and P. Müllner, Phys. Rev. Lett. **99**, 247201 (2007).
[9] R. Valdés Aguilar, A. B. Sushkov, S. Park, S.-W. Cheong, and H. D. Drew, Phys. Rev. B **74**, 184404 (2006).
[10] H. Fukumura, S. Matsui, J. Harima, T. Takahashi, T. Itoh, J. Kisoda, M. Tamada, Y. Noguchi, and M. Miyayama, J. Phys.: Condens. Matter **19**, 365224 (2007).
[11] T. Ruf, C. Thomsen, R. Liu, and M. Cardona, Phys. Rev. B **38**, 11985 (1988).
[12] A. B. Sushkov, J. L. Musfeldt, Y. J. Wang, R. M. Achey, and N.

S. Dalal, Phys. Rev. B **66**, 144430 (2002).
[13] R. Wesołowski, J. T. Haraldsen, J. Cao, J. L. Musfeldt, I. Olejniczak, J. Choi, Y. J. Wang, and J. A. Schlueter, Phys. Rev. B **71**, 214514 (2005).
[14] M. Rini, R. Tobey, N. Dean, J. Itatani, Y. Tomioka, Y. Tokura, R. W. Schoenlein, and A. Cavalleri, Nature (London) **449**, 72 (2007).
[15] J. Cao, L. I. Vergara, J. L. Musfeldt, A. P. Litvinchuk, Y. J. Wang, S. Park, and S.-W. Cheong, Phys. Rev. Lett. **100**, 177205 (2008).
[16] N. Hur, S. Park, P. A. Sharma, S. Guha, and S.-W. Cheong, Phys. Rev. Lett. **93**, 107207 (2004).
[17] C. R. dela Cruz, F. Yen, B. Lorenz, M. M. Gospodinov, C. W. Chu, W. Ratcliff, J. W. Lynn, S. Park, and S.-W. Cheong, Phys. Rev. B **73**, 100406(R) (2006).
[18] G. R. Blake, L. C. Chapon, P. G. Radaelli, S. Park, N. Hur, S.-W. Cheong, and J. Rodríguez-Carvajal, Phys. Rev. B **71**, 214402 (2005).
[19] B. Lorenz, Y.-Q. Wang, and C.-W. Chu, Phys. Rev. B **76**, 104405 (2007).
[20] S. C. Abrahams and J. L. Bernstein, J. Chem. Phys. **46**, 3776 (1967).
[21] W. Ratcliff, V. Kiryukhin, M. Kenzelmann, S. H. Lee, R. Erwin, J. Schefer, N. Hur, S. Park, and S. -W. Cheong, Phys. Rev. B **72**, 060407(R) (2005).
[22] D. Higashiyama, S. Miyasaka, N. Kida, T. Arima, and Y. Tokura, Phys. Rev. B **70**, 174405 (2004).
[23] S. Cheong and M. Mostovoy, Nat. Mater. **6**, 13 (2007).
[24] M. Mostovoy, Phys. Rev. Lett. **96**, 067601 (2006).
[25] G. D. Gale, J. Chem. Soc., Faraday Trans. **93**, 629 (1997).
[26] The interested reader may wonder if the peak structure near 710 cm^{-1} in Fig. 1(b) might be connected with symmetry breaking through the cascade of magnetic transitions. We believe it is not because (i) the peak is actually sitting in the background even at 300 K—far above T_{N1} and (ii) the peak does not show anomalies in either position or intensity across the phase-transition temperatures.
[27] C. Wang, G.-C. Guo, and L. He, Phys. Rev. Lett. **99**, 177202 (2007).
[28] C. Wang, G.-C. Guo, and L. He, Phys. Rev. B **77**, 134113 (2008).
[29] P. Allenspach, A. Furrer, and F. Hulliger, Phys. Rev. B **39**, 2226 (1989).
[30] A. A. Sirenko, S. M. O. Malley, K. H. Ahn, S. Park, G. L. Carr, and S.-W. Cheong, arXiv:cond-mat/0703255 (unpublished).
[31] M. Divis, J. Holsa, M. Lastrusaari, A. P. Litvinchuk, and V. Nekvasil, J. Alloys Compd. **451**, 662 (2008).
[32] M. Balkanski, R. F. Wallis, and E. Haro, Phys. Rev. B **28**, 1928 (1983).
[33] A. F. Garcíia-Flores, E. Granado, H. Martinho, R. R. Urbano, C. Rettori, E. I. Golovenchits, V. A. Sanina, S. B. Oseroff, S. Park, and S. –W. Cheong, Phys. Rev. B **73**, 104411 (2006).
[34] E. Granado, A. García, J. A. Sanjurjo, C. Rettori, I. Torriani, F. Prado, R. Sánchez, A. Caneiro, and S. B. Oseroff, Phys. Rev. B **60**, 11879 (1999).
[35] A. P. Litvinchuk, M. N. Iliev, V. N. Popov, and M. M. Gospodinov, J. Phys.: Condens. Matter **16**, 809 (2004).
[36] J. Laverdiére, S. Jandl, A. A. Mukhin, V. Yu. Ivanov, V. G. Ivanov, and M. N. Iliev, Phys. Rev. B **73**, 214301 (2006).
[37] W. Baltensperger and J. S. Helman, Helv. Phys. Acta **41**, 668 (1968).
[38] D. J. Lockwood and M. G. Cottam, J. Appl. Phys. **64**, 5876 (1988).
[39] C. J. Fennie and K. M. Rabe, Phys. Rev. Lett. **96**, 205505 (2006).
[40] A. B. Sushkov, O. Tchernyshyov, W. Ratcliff, S. W. Cheong, and H. D. Drew, Phys. Rev. Lett. **94**, 137202 (2005).
[41] In the paramagnetic phase, $\langle \mathbf{S}_i \cdot \mathbf{S}_j \rangle$ is primarily spin diffusion [for three-dimensional (3D) systems] and is defined by a temperature-dependent correlation length. In the critical regime, it is defined by scaling functions. Well into the ordered phase, the spin-spin correlation function describes spin waves.
[42] A. B. Sushkov, R. V. Aguilar, S. Park, S. -W. Cheong, and H. D. Drew, Phys. Rev. Lett. **98**, 027202 (2007).
[43] The development of a large, dropping background near 120 cm^{-1} complicates the latter picture somewhat, resulting in larger error bars. This background may arise because these features are stealing oscillator strength from the cluster of excitations between 140 and 180 cm^{-1} (Ref. 9).